J Appl Electrochem (2012) 42:179–187
DOI 10.1007/s10800-012-0386-4

ORIGINAL PAPER

Application of nanocrystalline graphite-like pyrolytic carbon film electrode for voltammetric sensing of lead

Mojtaba Hadi · Ahmad Rouhollahi · Mohammad Yousefi

Received: 17 November 2011 / Accepted: 20 January 2012 / Published online: 4 February 2012

Abstract A nanocrystalline pyrolytic carbon film was employed as working electrode to detect micromolar-level concentrations of lead by anodic stripping voltammetery as an example of its potential applications in environmental analysis. The response was compared with conventional carbon-based electrodes such as glassy carbon, edge-plane pyrolytic graphite, and basal-plane pyrolytic graphite electrodes. The favorable properties of this carbon coating for Pb detection lie in its high degree of sensitivity, high response stability, low memory effect, and a good repeatability. The applicability of this sensor was tested on spiked tap water and river water samples.

Keywords Pyrolytic carbon film · Carbon nanostructures · Lead · Anodic stripping voltammetry · Edge-plane sites

Abbreviations

ASV	Anodic stripping voltammetery
BDD	Boron-doped diamond-like
BPPG	Basal-plane pyrolytic graphite
CNT	Carbon nanotube
CVD	Chemical vapor deposition
DOS	Density of states
DPASV	Differential pulse anodic stripping voltammetry
EPPG	Edge-plane pyrolytic graphite
FTIR	Fourier transform infrared
FWHM	Full-width at half-maximum
GC	Glassy carbon
NDD	Nitrogen-doped diamond-like
PCF	Pyrolytic carbon film
RSD	Relative standard deviation
S/B	Signal-to-background
SEM	Scanning electron microscope
XPS	X-ray photoelectron spectroscopy
XRD	X-ray diffraction

M. Hadi · A. Rouhollahi (✉)
Department of Chemistry, Faculty of Sciences, K.N. Toosi University of Technology, No. 41, Kavian St., Mojtabaee St., Seyyed Khandan Bridge (N.), Shariati Ave., P.O. Box 16315-1618, 15418-49611 Tehran, Iran
e-mail: rouhollahi@kntu.ac.ir

M. Yousefi
Department of Petrochemicals, Iran Polymer and Petrochemical Institute, Tehran, Iran

1 Introduction

Lead is one of the specific classes of metals that can be described as highly toxic. Considering its damaging effects on human health and environment [1], the determination of trace lead is very important. Anodic stripping voltammetery (ASV) is recognized as an effective technique for detection of trace levels of heavy metals because of remarkably low detection limits, sensitivity, and specificity [2, 3]. Although in the past years, hanging drop mercury and mercury-coated electrodes [4–6] have been successfully employed in ASV for metal ion detection, still there is a need to develop alternate electrodes because of toxicity, volatility, high background current, and difficulties in the determination of metals with stripping potentials more positive than that of mercury. Bi-modified or Bi-based composite modified electrodes have been used successfully as the alternatives, with comparable or superior performance than those of mercury or other alternate metal-based electrodes such as Ir, Ag, and Au [7–10]. However, a low anodic potential limit and in some cases a high limit of detection is probably the major drawbacks associated with Bi-based modified electrodes [11].

Among the existing solid electrodes, some efforts are made on the development of structured carbon-based electrodes due to their wide potential windows, low background current, chemical inertness, and ease of use [12, 13]. Recently, several types of new nanostructured carbon-based materials have been employed successfully for metal ions detection. For example, a multi-wall carbon nanotube (CNT)-modified glassy carbon (GC) electrode has been used for lead detection and exhibited higher sensitivity compared with bare GC electrode [14]. The reason for such excellent electroactivity lies in CNTs high specific surface area and high density of electrochemically active edge-planes that occur at the open ends or defect sites of tubes [12, 13, 15], though the CNTs preparation as a time-consuming procedure and large residual currents may be their major drawbacks [16]. More recently, CNT-based composite-modified electrodes have also been used successfully in ASV for lead ions detection [17–19]. Another example is nanocrystalline diamond-like thin films doped with boron or nitrogen that have received considerable attention as electrode materials for metal ion detection [20–22]. They may be considered as better alternatives to CNT-modified electrodes due to their wide potential windows, lower background currents, and improved signal-to-background (S/B) ratios [23]. Comparing the results from ASV analysis using a boron-doped diamond-like (BDD) electrode with those of mercury electrode, the BDD electrode in general exhibits the detection figures superior to those of mercury [24]. Edge-plane pyrolytic graphite (EPPG) is another alternative carbon-based electrode that has been investigated during the last few years [12, 25]. Compton and co-workers have studied this electrode for ASV detection of some metal ions and found that the performance of EPPG electrode is superior in terms of sensitivity, detection limit, and reproducibility compared to carbon paste and BDD electrode [25–27]. Under the same conditions, it shows three times higher sensitivity compared to BDD electrode [26]. The favorable properties of EPPG have been attributed to its surface consisting entirely of active edge-plane sites that act as nucleation sites for the growth of metal on the pre-concentration step of ASV analysis [12, 15, 27].

More recently, graphene-based nanomaterials, one of the most recent members of carbon nanostructures family, have proved to be an ideal for applications in electroanalysis [28]. Graphene-modified [29] and graphene-based composite electrodes [30] have shown excellent performance for metal ion detection. The solvent dispersion and subsequent casting of graphene onto the surface of electrode substrate is a routine method used for the preparation of graphene-based modified electrodes [29–32]. However, a high residual current due to their large surface area, poor mechanical stability, and weak adhesion of solvent-cast carbon film onto the surface of substrate may be the major drawbacks associated with carbon film electrodes prepared by solvent-casting method.

Pyrolytic carbon films (PCFs), nanostructured forms of carbon belonging to the above groups, have been reported as new and attractive electrode materials for electroanalytical applications [33–36]. The structure is composed of two-dimensional hexagonal graphitic sheet aggregates with more or less preferential orientation to the substrate surface, depending on the chemical vapor deposition (CVD) processing conditions [37–39]. The small size of graphene layers (1–3 nm) is the reason why this carbon film provides a very high fraction of electrochemically active edge sites on the surface [35, 36]. High mechanical stability, strong adhesion to the surface of carbon-based substrates, low level of porosity, surface smoothness, and low capacitive current [34–36, 38, 39] may be considered as the major advantages of these CVD-prepared graphene films over the modified electrodes prepared by solvent-casting technique.

To the best of our knowledge, determination of trace heavy metals based on bare PCF electrode has not been reported. This study was primarily aimed at evaluating the ability and potential applications of mercury-free PCF electrode for detecting lead within the micromolar concentration range by using differential pulse anodic stripping voltammetry (DPASV). The analytical response is compared under the same conditions with EPPG, GC, and basal-plane pyrolytic graphite (BPPG) electrodes. The results confirm that PCF can be a suitable electrode material that provides comparable or superior electroanalytical response. This is followed by a discussion on the possibility of determining trace levels of lead in tap and river water samples.

2 Materials and methods

2.1 Carbon film preparation

PCFs were deposited on graphite rods (3.9 mm diameter, 5 mm height) in a hot-wall CVD reactor that consisted of a quartz tube heated by a vertical tube furnace [34]. For all carbon coating runs, methane gas was used as a carbon source with argon as a carrier gas with an optimum flow rate of 50 cm^3 min^{-1} for methane and 50 cm^3 min^{-1} for argon. The flow rates were measured and controlled with electronic mass flow controllers with a measurement accuracy of about ± 1.5 cm^3 min^{-1}. The total pressure was ambient and the depositions were performed at an optimum temperature of 1,100 °C [35], which was regulated with a thermocouple located at the central part of the reactor tube and a PID temperature controller. The isothermal zone was

10-cm high within a temperature range of ±5 °C. The deposition duration was 90 min.

2.2 Electrochemical measurements

To prepare the PCF electrode, the side wall of the graphite rods with carbon coating was encased in heat-shrinkable tubing. Silver paste was placed on top of the graphite rods and a copper wire was used to complete the electrical connection. The working electrode geometry was thus a planar disk of 3.9-mm diameter. Electrochemical experiments were performed with an Autolab potentiostat (PGSTAT30) with a three-electrode configuration. All potentials are reported with respect to an Ag/AgCl (3 M KCl) reference electrode and a graphite rod was used as the counter electrode. To compare the cyclic voltammograms, GC (2-mm diameter), BPPG, and EPPG electrodes were used as working electrodes. The GC electrode was prepared by polishing with successive slurries of 1.0 and 0.05 μm alumina on a polishing cloth and finally sonicated in distilled water for 10 min. The EPPG and BPPG electrodes were prepared from pyrolytic graphite pieces machined into 2.4-mm-diameter disks, with the faces parallel with the edge-plane or basal-plane [12]. The EPPG electrode was first polished on several emery polishing papers of coarser size to finer size to obtain a smooth surface and then treated in the same manner as described above for the GC [26, 27]. The surface of BPPG was renewed by pressing a strip of cellotape onto the electrode surface and peeling away the top few layers of graphite [12]. All solutions were made from analytical grade reagents and Milli-Q ultrapure water. Before each measurement, the cell content was de-aerated by passage of nitrogen bubbles for 5 min. During the deposition step, the solution was stirred, and following a 10-s equilibration period, the stripping step was performed under undisturbed conditions.

2.3 Carbon film characterization

Carbon coatings were examined by a Cambrige-S360 scanning electron microscope (SEM), observing the surface or the side view of the coating's fractured surface. The crystallite size was determined using X-ray diffraction (XRD) with a laboratory X-ray powder diffractometer (D8 Advance, Bruker AXS) at 40 kV and 40 mA with copper K_α radiation. A quartz sample was used as a standard for calibration. For XRD measurements, carbon coating was stripped from the graphite rod, ground to powder, and finally poured in sample holder. The specific surface area of the graphite substrate and coated graphite substrate were measured using the BET method (CHEMBET, Quantachrom, 3000).

3 Results and discussions

3.1 SEM and BET analysis

The SEM images of the surface and cross-section view of fractured surface of the PCF are shown in Fig. 1. Figure 1a shows the layered structure of the PCF. Porous graphite surface, covered entirely by well-bonded thin matrix carbon layers which are oriented parallel to the surface of substrate, can be recognized in this figure. Figure 1b shows the surface morphology of the carbon film, and Fig. 1c shows a higher magnification view of the surface. The cell-like globular morphology of the surface (Fig. 1b, c) is very similar to that observed for PCF deposited on cordierite substrate [40, 41], which may be induced by grains elongated along the bulk of the carbon film [40]. Based on studies by several research groups, there is a complex correlation between the structural properties of PCF and the deposition conditions [37, 42, 43]. The selected CVD conditions in this study, as given in the experimental section, deposit a smooth and continuous carbon film with a dense laminar structure [35]. A smooth surface without any indication of fractures, defects, or porosities on the surface (Fig. 1b, c) as well as beneath the surface plane possibly results from the laminar structure of the carbon film (Fig. 1a).

The specific surface area of the graphite substrate was about 0.24 $m^2\ g^{-1}$. After carbon film deposition, the surface area considerably decreased to a value as small as about 0.09 $m^2\ g^{-1}$. As it may be seen in Fig. 1a, the graphite substrate has many pores and it may be considered that these pores could be filled with the carbon deposits that cover entirely the surface of graphite substrate during the coating process. Dense and laminar carbon coating with a smooth crack-free surface effectively prevents the penetration of gases and liquids into the deeper parts.

3.2 XRD analysis

As expected, a sharp (002) diffraction line at 2θ of 25.4° in the XRD diffraction patterns (Fig. 2) is an indication of the crystalline nature of PCF. The structure may be viewed as aggregates of graphite crystallites, each of which consists of some graphene sheets stacked together [37]. From the (100) diffraction line at 2θ of 43° and applying the Scherrer equation ($L = 0.9\ \lambda/\beta\ \cos\ \theta$), where λ is the wavelength of radiation, θ is the Bragg angle, and β is the full-width at half-maximum (FWHM) of the diffraction peak, the average size of graphene sheets, L_a, may be estimated [44] to be about 3.5 nm, which corresponds more or less to that measured by Raman spectroscopy [34]. To obtain the β value, the (100) diffraction line was fitted with Gaussian distribution function (inset of Fig. 2). The graphitic nature

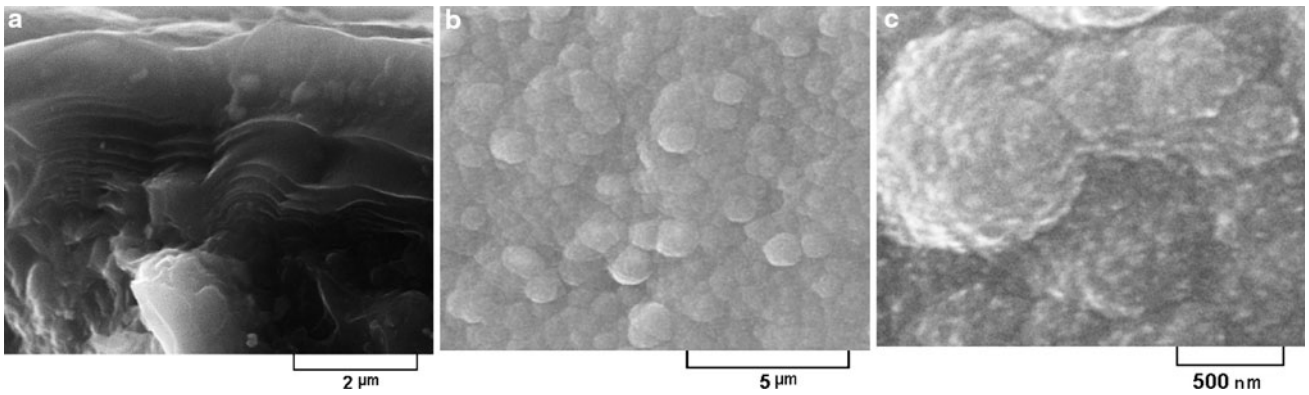

Fig. 1 Typical SEM images at a magnification of 5,000 (**a**) of the side view of fractured surface and at a magnification of 5,000 (**b**) and 30,000 (**c**) of the surface of PCF

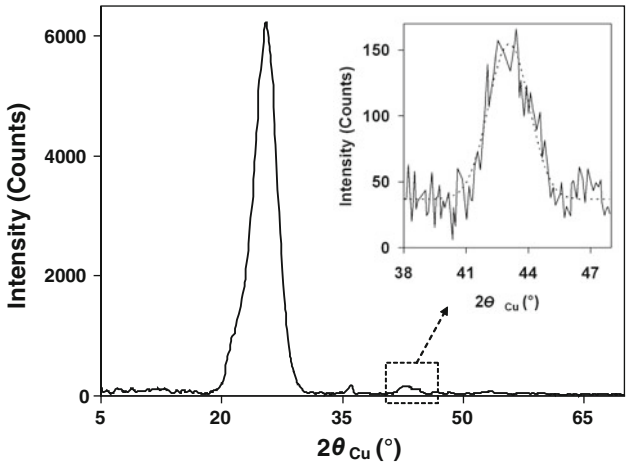

Fig. 2 XRD pattern of PCF. *Inset* shows the (100) diffraction line (*solid line*) fitted with Gaussian distribution function (*dotted line*)

of the PCF is inherently for a more uniform and higher electrical conductivity compared to non-uniform electrical conductivity observed at the BDD film [45]. The XRD results (small graphitic crystallites) as well as the lamellar structure, shown in the SEM micrographs, could be the explanation for a high fraction of surface active edge sites and surface smoothness. Such conductive carbon film can be used successfully as electrode materials.

The other factor that must be considered is the surface chemistry that plays an important role in electrochemical properties of carbon electrodes [13]. The processing gases such as methane and argon used for carbon film deposition create a surface composed of a large amount of sp^2-hybridized carbon atoms and a low amount of hydrogen atoms [38, 44]. Also, it has been shown that the surface of carbon materials is prone to react spontaneously with atmospheric oxygen to form surface oxide functional groups that change its chemical nature and affect its electrochemical performances [13]. Examination of the existence of surface oxide functional groups with Fourier transform infrared (FTIR) spectroscopy [36] and X-ray photoelectron spectroscopy (XPS) method [33] indicate the presence of a low amount of carbonyl and hydroxyl functional groups on the surface of the PCF electrode.

3.3 DPASV of lead at the PCF electrodes and comparing the responses with other unmodified carbon-based electrodes

Our study was primarily focused on the anodic stripping response of PCF electrode compared with that of GC, EPPG, and BPPG electrodes for the determination of lead. Figure 3 shows the overlaid DPASV curves for Pb^{2+} obtained under the same conditions, enabling the direct comparison of some of the figures of merit for each electrode that are summarized in Table 1. From Fig. 3, it can be seen that the response at the PCF is higher than that at the GC electrode, which can be attributed to the surface structural properties of PCF electrode. The role of surface density of active edge sites on the stripping current of Pb can be clarified by comparing the response of PCF electrode with that of EPPG and BPPG electrodes. Larger voltammetric response at the EPPG (Fig. 3) compared to that observed at the BPPG electrode can be attributed to the surface structure of EPPG that consists solely of active edge sites that provide more nucleation sites for the growth of solid lead nuclei compared to the BPPG surface with a low proportion of edge sites and a high amount of electrochemically inert basal planes [12, 15, 25–27]. Comparing the response of PCF electrode to that of EPPG electrode, it may be suggested that a high fraction of surface edge sites could be the reason for PCF exhibiting a high sensitivity comparable to that of EPPG, resulting from PCF small graphitic crystallites that provide a surface with a high edge/basal ratio [35, 36]. Another important parameter of merit is the background current as a low noise/background current combined with a high sensitivity

enabling a superior limit of detection values to be achieved. As the background curves in Fig. 3 show, the PCF electrode has a lower background current compared to EPPG and GC electrodes. Due to the low density of states (DOS) of BPPG [13], this electrode has the lowest residual current (Table 1) but it is offset by its low sensitivity. The lower background current of the PCF electrode due to surface smoothness combined with its high sensitivity can lead to the determination with an enhanced limit of detection. The stripping peak potential value for each electrode is also presented in Table 1. The peak potentials are approximately the same at both PCF and EPPG electrodes but the slightly more positive values at BPPG and GC electrodes may be a reflection of their more sluggish electron transfer kinetics. The values of full-width at half-maximum (FWHM) of the stripping peak at each electrode are also presented in Table 1. The values of FWHM at GC, BPPG, and EPPG electrodes are nearly similar and are slightly larger than the corresponding value at PCF electrode. Probably, the surface smoothness, uniformity, and surface electrochemical homogeneity as discussed earlier lead to a narrower peak at PCF electrode with a FWHM value that is close to the value observed at the Hg-coated GC electrode [24]. The narrower peaks are desired because a better resolution can be obtained for analysis of multiple metal ions. Another important analytical parameter is the reproducibility, which is affected mainly by the cleaning performance of the electrode [46]. The cleaning performance was assessed in accordance with Liu's report [46] by considering the formula of $I_{remain}/(I_{remain} + I_{strip})$, in which I_{strip} is the stripping peak current obtained by scanning in a 3 μM solution of Pb followed by removing the adsorbed ions by dipping the electrode in distilled water for 3 min and then scanning again in the supporting electrolyte solution without Pb ions to obtain I_{remain}. The fraction of the remaining Pb on the PCF electrode surface was calculated to be 5% that is lower than that observed at the GC electrode of about 10.9% and the other carbon electrodes of this study (Table 1). It was suggested that a low cleaning performance of GC electrode may be attributed to metal ion entrapped at the surface defects during the metal ion deposition step [46]. Thus, a high cleaning performance of PCF electrode may be attributed to its surface structure, as checking the surface or side view of the fractured surface of PCF coating (Fig. 1) confirmed a relatively defect-free structure. The reproducibility was assessed from run-to-run and from electrode-to-electrode. The relative standard deviation (RSD) of peak heights for five stripping cycles of Pb was below 3.5%. This shows that the reproducibility of PCF is comparable with that of nitrogen-doped diamond-like (NDD) film (2.0%) [47], BDD (3.8%) [24], Hg-coated GC (3.6%) [24], and Hg-coated diamond-like film (0.5–5%) electrodes [48]. Also, the electrode-to-electrode reproducibility was excellent with an RSD value of below 4% for ten PCF electrodes prepared in one batch or below 6% for five PCF electrodes prepared under the same conditions but in five separate batches of CVD. This result indicates that, by suitable adjustment and carefully controlled CVD processing parameters, as mentioned in the experimental section, carbon films can be fabricated with excellent reproducibility toward the determination of Pb.

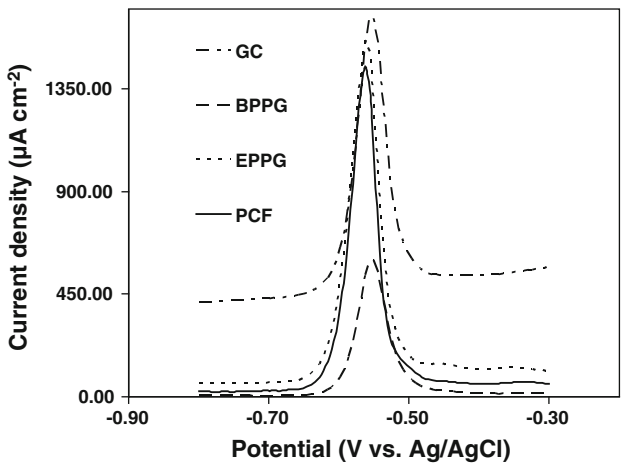

Fig. 3 Overlaid DPASV curves for a 1 μM solution of Pb ion in 0.1 M KCl (pH 1.0) at PCF (*solid line*), BPPG (*dashed line*), EPPG (*dotted line*), and GC (*dotted-dashed line*). The deposition potential was −1.3 V and the deposition time was 180 s with solution stirred at 900 rpm. All curves are uncorrected for the background current. The waveform parameters are given in the text

3.4 Evaluation and optimization of conditions for lead analysis

Further studies were carried out to investigate the optimum conditions for ASV determination of lead. The effect of potential scan parameters of DPASV mode on the peak height and background current was investigated and it was found that the step potential of 6 mV, interval time of 0.2 s, modulation amplitude of 100 mV, and modulation time of 0.01 s are optimum waveform parameters to achieve a high S/B ratio. Figure 4 shows the effect of deposition potential on the response of PCF electrode and the inset a in this figure shows the plot of peak current versus the applied deposition potential. As it is evident from this figure, the stripping peaks of Pb increase when deposition potential decreases probably due to a rise in the mobility of Pb ion from the bulk solution to the surface of electrode, leading to an increase in the amount of Pb deposited on the surface [49, 50]. At the voltage of about −1.3 V, a maximum peak current is obtained and further decrease in applied voltage results in weaker response. A similar behavior was also observed at NDD electrode [47] and nitrogen-doped tetrahedral amorphous carbon film

Table 1 Stripping peak current, background current, peak potential, FWHM, and cleaning performance for PCF, GC, EPPG, and BPPG electrodes in the presence of 1 μM Pb ion

Electrode	Peak current[a] ($\mu A\ cm^{-2}$)	Background at peak potential[a] ($\mu A\ cm^{-2}$)	Peak potential[a] (mV vs. Ag/AgCl)	FWHM[a] (mV)	Cleaning performance (%)
PCF	127 ± 4	3.54 ± 0.21	–562 ± 3	42 ± 2	5.1
GC	103 ± 8	44.02 ± 3.41	–554 ± 2	48 ± 2	10.9
EPPG	131 ± 6	8.02 ± 0.36	–562 ± 4	48 ± 2	8.8
BPPG	51 ± 4	0.90 ± 0.08	–551 ± 2	48 ± 1	6.2

[a] Mean and standard deviation values of five repeated measurements

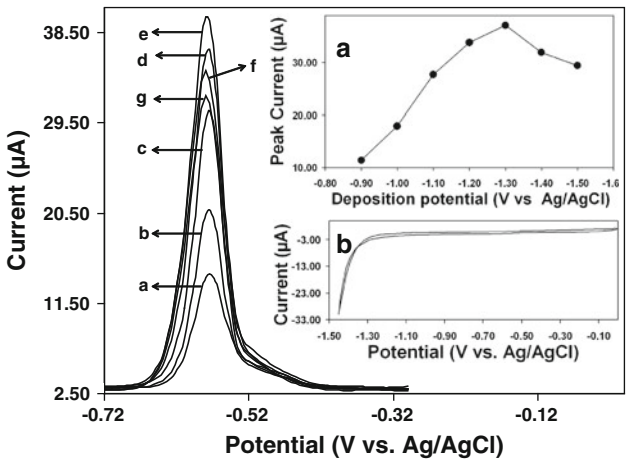

Fig. 4 Effect of deposition potential on the stripping response of the PCF electrode in a 0.5 μM solution of Pb in 0.1 M KCl (pH 1.0). Deposition potentials are −0.9 (a), −1.0 (b), −1.1 (c), −1.2 (d), −1.3 (e), –1.4 (f), and –1.5 V (g). Other conditions are as in Fig. 3. *Inset a* shows the plot of peak current versus the applied deposition potential, and *inset b* shows the cathodic direction of cyclic voltammogram in the supporting electrolyte solution at the scan rate of 50 mV s^{-1}

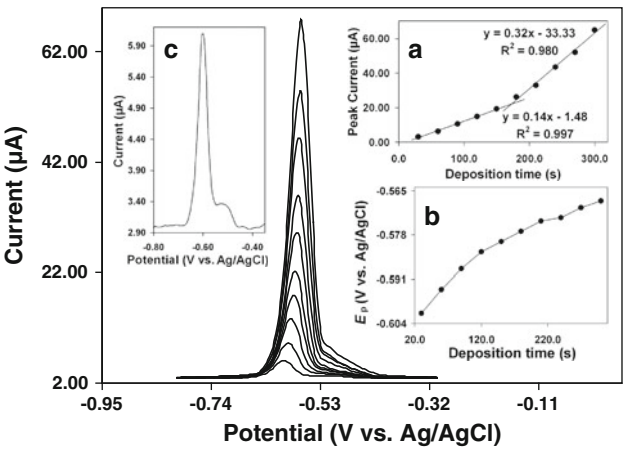

Fig. 5 Effect of deposition time on the stripping response of the PCF electrode in a 0.3 μM solution of Pb in 0.1 M KCl (pH 1.0). Deposition times from bottom to top are 30, 60, 90, 120, 150, 180, 210, 240, 270, and 300 s. Other conditions are as in Fig. 3. *Inset a* shows the plot of peak current versus the deposition time. *Inset b* shows the plot of stripping peak potentials (E_p) versus the deposition time. *Inset c* shows a closer view of the first voltammogram (deposition time of 30 s)

electrode [49, 50], which was attributed to hydrogen evolution that diminishes the normal diffusion of metal ions toward the surface of electrode. From the cathodic direction of background cyclic voltammogram in supporting electrolyte (inset b), the onset of hydrogen evolution is at the voltage of about −1.3 V, which is consistent with the results from inset a. Figure 5 shows the effect of the deposition time on the stripping response of PCF electrode and the plot of peak current versus the deposition time is shown in inset a. An increase of the deposition time leads to a linear increase of the peak current but at deposition time beyond 180 s, a change in the slope was observed. This behavior has also been observed at some other carbon-based electrodes [51], attributed to a change in deposited film structure and formation of more compact Pb lattice after some critical film thickness. Inset b shows that the stripping peak potential of Pb shifts to less negative values with increased deposition time, which can be correlated to the increased concentration of stripped Pb ions by applying the Nernst equation [49, 50]. Closer inspection of the baseline (inset c) shows the presence of another stripping peak at about −509 mV. This peak has also been observed at some other carbon-based electrodes [51, 52], attributed to stripping of lead nuclei from the bare surface of carbon electrode, whereas the peak at less positive potential (*ca.* −598 mV) can be related to stripping of lead from lead nucleation centers.

3.5 Detection figures of merit

Figure 6 shows the DPASV responses under the optimum conditions for successive standard additions of Pb ion. From the analysis of the peak height versus Pb concentration, linear relations between two different regions were observed, as shown in the inset of Fig. 6. Similar to that suggested for the effect of deposition time as stated above, this behavior could be explained again by the formation of compacted Pb deposits above some critical

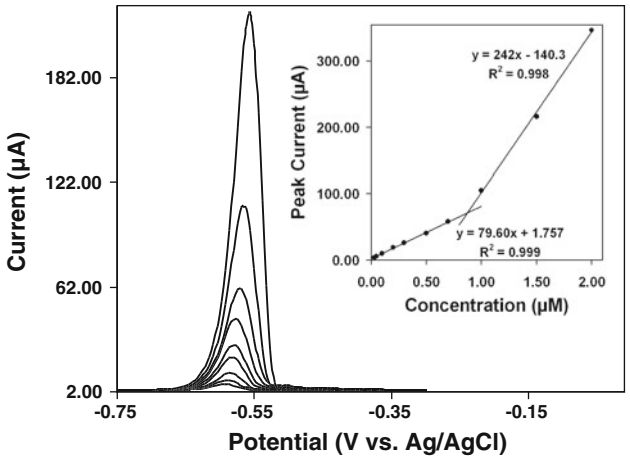

Fig. 6 Effect of Pb concentration on the stripping response of PCF electrode in 0.1 M KCl (pH 1.0). Concentrations from bottom to top are 0.03, 0.05, 0.1, 0.2, 0.3, 0.5, 0.7, 1.0, 1.5, and 2.0 μM. Other conditions are as in Fig. 3. *Inset* shows the corresponding calibration curve

film thickness [51]. Over the lower concentration range of 0.03–0.7 μM, the peak current increases linearly with a correlation coefficient of about 0.9987 and a sensitivity of about 79.6 μA μM^{-1}. The detection limit (based on signal-to-background ratio of 3) was found to be 0.009 μM although with a deposition time longer than 180 s, a lower detection limit and a higher sensitivity could be expected. Table 2 compares some analytical figures of merit of the PCF electrode to those of some mercury-free structured carbon-based electrodes and an Hg–GC electrode, which shows that the detection limit, dynamic range, and sensitivity for DPASV are comparable to or in some cases even slightly better than those in the literature.

3.6 Interference study

The possible interferences of some inorganic species with the detection of a trace amount of lead were also tested. The results indicate that cations such as Na^+, K^+, Ca^{2+}, Mg^{2+}, Zn^{2+}, Fe^{2+}, Al^{3+}, Cu^{2+}, and Cd^{2+} (10 μM) and anions such as F^-, Cl^-, Br^-, $SO4_2^-$, and NO_3^- (10 μM) have negligible interference on the signals of Pb^{2+} and the changes in the stripping signal of Pb (0.5 μM) after addition of each cation or anion were below 4%. Figure 7 shows typical voltammograms of 0.7 μM Pb^{2+} before (solid line) and after addition of 1 μM Cu^{2+} (dashed line), 10 μM Cd^{2+} (dotted line), and then 30 μM Zn^{2+} (dashed-dotted line). As it is clear from this figure, the main peak of Pb remains constant and only Cu^{2+} makes the −0.50 peak, as discussed earlier (inset c of Fig. 5), to be increased. A similar effect has been observed at the screen-printed carbon film electrode [51].

3.7 Application to real environments

The efficiency of the PCF electrode in practical analysis was assessed in the determination of Pb in some natural water samples (tap water and river water) by standard

Table 2 A comparison between analytical figures of merit of PCF electrode and some mercury-free structured carbon-based electrodes and Hg–GC electrode for DPASV determination of Pb ions

Electrode	Conditions	Linear dynamic range (μM)	Detection limit (μM)	Sensitivity (μA μM^{-1})	Reference
PCF electrode	0.1 M KCl (pH 1.0), deposition time 180 s, deposition potential −1.30 V (vs. Ag/AgCl)	0.03–0.8	0.010	79.6	This study
GC electrode modified with multi-wall carbon nanotubes	0.1 M acetate buffer (pH 4.5) containing 0.02 mol/l KI, deposition time 300 s, deposition potential −1.20 V (vs. SCE)	0.02–10	0.004	20.9	14
Nanocrystalline boron-doped diamond electrode	0.1 M acetate buffer, deposition time 60 s, deposition potential −1.7 V (vs. SCE)	0.037–0.483	0.011	19.4	20
Boron-doped diamond electrode	0.1 M acetate buffer (pH 5.2), deposition time 210 s, deposition potential −0.800 V (vs. Ag/AgCl)	0.024–4.83	0.024	2.69	24
Hg–GC electrodes	0.1 M acetate buffer (pH 5.2), deposition time 210 s, deposition potential −0.800 V (vs. Ag/AgCl)	0.024–4.83	0.024	7.23	24
Nitrogen-doped diamond-like carbon film	0.1 M KCl (pH 1.0), deposition time 120 s, deposition potential −1.00 V (vs. SCE)	0.5–2	0.076	–	47
Screen-printed carbon electrode	0.1 M HCl, deposition time 150 s, deposition potential −1.4 V (vs. SCE)	0.024–0.116	0.012	67.1	51

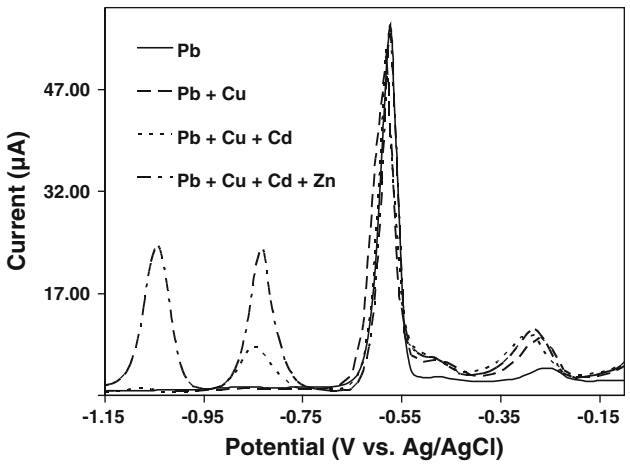

Fig. 7 Stripping voltammograms at PCF electrode in a 0.7 μM solution of Pb in 0.1 M KCl (pH 1), before (*solid line*) and after addition of 1 μM Cu^{2+} (*dashed line*), 10 μM Cd^{2+} (*dotted line*), and 30 μM Zn^{2+} (*dashed-dotted line*). Other conditions are as in Fig. 3

Table 3 Result of quantitative determination of Pb in different water samples spiked with a known quantity of Pb

Sample	Pb added (μM)	Pb found[a] (μM)	RSD (%)	Recovery (%, $n = 5$)
Tap water				
1	0.100	0.097	3.2	97
2	0.300	0.302	2.8	101
3	0.500	0.503	3.1	101
River water				
1	0.100	0.103	2.9	103
2	0.200	0.198	3.1	99
3	0.500	0.505	2.8	101

[a] Average of five determinations

addition method. Recovery test was carried out by spiking known amounts of standard in the sample matrix to assess the accuracy. The samples were acidified to pH 1 with HCl immediately after the sample collection. The results are given in Table 3. The good recoveries demonstrate the reliability of using the PCF electrode for determination of Pb in natural water samples.

4 Conclusions

The stripping voltammetric determination of trace levels of lead utilizing a mercury-free nanocrystalline PCF electrode has been demonstrated in this study. The response of the PCF electrode, as compared under the same conditions with those of EPPG, BPPG, and GC electrodes, has been shown to be superior with a high sensitivity, good cleaning performance, repeatability, and improved signal-to-noise characteristics. These favorable features are likely derived from PCF surface structural properties, high density of states, uniformity, and surface smoothness. The preconcentration parameters were optimized and the calibration graph of Pb shows a good linear relationship from 0.03 to 0.7 μM and a slope of 79.6 μA μM^{-1}. The PCF electrode exhibits good applicability for the detection of lead in tap water and river water samples. Low residual current, high structural stability, and strong adhesion to the surface of graphite substrate may be mentioned as the advantages of CVD-prepared PCF electrodes over the graphene-based carbon films prepared by solvent-casting technique. The other advantages that should be considered are simple and low-cost non-catalytic CVD technique and the possibility of fabricating more than 70 PCF electrodes per each run of the CVD process that prorates considerably the fabrication costs for each electrode.

References

1. Flick DF, Kraybill HF, Dimitroff JM (1971) Environ Res 4:71
2. Aldstadt JH, Dewald HD (1992) Anal Chem 64:3176
3. Wang J (1985) Stripping analysis: principles, instrumentation and applications. VCH, Deerfield Beach
4. Economou A, Fielden PR (2003) Analyst 128:205
5. Sherigara BS, Shivaraj Y, Mascarenhas RJ, Satpati AK (2007) Electrochim Acta 52:3137
6. Gustavson I, Lundström K (1983) Talanta 30:959
7. Wang J, Lu JM, Hocevar SB, Farias PAM, Ogorevc B (2000) Anal Chem 72:3218
8. Hocevar SB, Daniele S, Bragato C, Ogorevc B (2007) Electrochim Acta 53:555
9. Armstrong C, Tatum CE, Dansby-Sparks RN, Chambers JQ, Xue ZL (2010) Talanta 82:675
10. Pauliukaite R, Hocevar SB, Ogorevc B, Wang J (2004) Electroanalysis 16:719
11. Korolczuk M, Moroziewicz A, Grabarczyk M (2005) Anal Bioanal Chem 382:1678
12. Banks CE, Compton RG (2006) Analyst 131:15
13. McCreery RL (2008) Chem Rev 108:2646
14. Wu K, Hu S, Fei J, Bai W (2003) Anal Chim Acta 489:215
15. Banks CE, Moore RR, Davies TJ, Compton RG (2004) Chem Commun 16:1804
16. Poh WC, Loh KP, Zhang WD, Triparthy S, Ye JS, Sheu FS (2004) Langmiur 20:5484
17. Wang Z, Liu E, Gu D, Wang Y (2011) Thin Solid Films 519:5280
18. Hwang GH, Han WK, Park JS, Kang SG (2008) Talanta 76:301
19. Ouyang R, Zhu Z, Tatum CE, Chambers JQ, Xue Z (2011) J Electroanal Chem 656:78
20. Sonthalia P, McGaw E, Show Y, Swain GM (2004) Anal Chim Acta 522:35
21. Tall OE, Jaffrezic-Renault N, Sigaud M, Vittori O (2007) Electroanalysis 19:1152
22. Hian C, Grehan KJ, Goeting CH, Compton RG, Foord JS, Marken F (2003) Electroanalysis 15:169
23. Compton RG, Foord JS, Marken F (2003) Electroanalysis 15:1349
24. McGaw EA, Swain GM (2006) Anal Chim Acta 575:180
25. Banks CE, Compton RG (2005) Anal Sci 21:1263

26. Welch CM, Banks CE, Komorsky-Lovrić Š, Compton RG (2006) Croat Chem Acta 79:27
27. Wantz F, Bank CE, Compton RG (2005) Electroanalysis 17:655
28. Pumera M, Ambrosi A, Bonanni A, Chng ELK, Poh HL (2010) Trends Anal Chem 29:954
29. Wang B, Chang Y, Zhi L (2011) New Carbon Mater 26:31
30. Li J, Guo S, Zhai Y, Wang E (2009) Anal Chim Acta 649:196
31. Goh MS, Pumera M (2010) Electrochem Commun 12:1375
32. Goh MS, Pumera M (2010) Chem Asian J 5:2355
33. Keeley GP, McEvoy N, Kumar S, Peltekis N, Mausser M, Duesberg GS (2010) Electrochem Commun 12:1034
34. Hadi M, Rouhollahi A, Yousefi M, Taidy F, Malekfar R (2006) Electroanalysis 18:787
35. Hadi M, Rouhollahi A, Yousefi M (2011) Electroanalysis 23:1497
36. Hadi M, Rouhollahi A, Yousefi M (2011) Sens Actuators B 160:121
37. De Pauw V, Reznik B, Kalhöfer S, Gerthsen D, Hu ZJ, Hüttinger KJ (2003) Carbon 41:71
38. Hüttinger J (2003) In: Delhaès P (ed) Fibers and composites (world of carbon). Taylor and Francis, London, p 75
39. Oberlin A (2002) Carbon 40:7
40. Reznik B, Norinaga K, Gerthsen D, Deutschmann O (2006) Carbon 44:1298
41. Brüggert M, Hu Z, Hüttinger KJ (1999) Carbon 37:2021
42. Hu ZJ, Zhang WG, Hüttinger KJ, Reznik B, Gerthsen D (2003) Carbon 41:749
43. De Pauw V, Kalhöfer S, Gerthsen D (2004) Carbon 42:279
44. Vallerot J, Bourrat X, Mouchon A, Chollon G (2006) Carbon 44:1833
45. Holt KB, Bard AJ, Show Y, Swain GM (2004) J Phys Chem B 108:15117
46. Wang Z, Liu E, Zhao X (2011) Thin Solid Films 31:5285
47. Zeng A, Liu E, Tan SN, Zhang S, Gao J (2002) Electroanalysis 14:1294
48. Xu J, Granger MC, Chen Q, Strojek JW, Swain GM (1997) Anal Chem 69:591A
49. Khun W, Liu E (2009) Electrochim Acta 54:2890
50. Khun NW, Liu E (2009) Thin Solid Films 518:4003
51. Honeychurch KC, Hart JP, Cowell DC (2000) Electroanalysis 12:171
52. Babyak C, Smart RB (2004) Electroanalysis 16:175